Imaging Mass Spectrometry and Proteome Analysis of Marek's Disease Virus-Induced Tumors

V. I. Pauker,[a] L. D. Bertzbach,[b] A. Hohmann,[a] A. Kheimar,[b,c] J. P. Teifke,[d] T. C. Mettenleiter,[a] A. Karger,[a] B. B. Kaufer[b]

[a]Institute of Molecular Virology and Cell Biology, Friedrich-Loeffler-Institut, Greifswald-Insel Riems, Germany
[b]Institute of Virology, Freie Universität Berlin, Berlin, Germany
[c]Department of Poultry Diseases, Faculty of Veterinary Medicine, Sohag University, Sohag, Egypt
[d]Department of Experimental Animal Facilities and Biorisk Management, Friedrich-Loeffler-Institut, Greifswald-Insel Riems, Germany

ABSTRACT The highly oncogenic alphaherpesvirus Marek's disease virus (MDV) causes immense economic losses in the poultry industry. MDV induces a variety of symptoms in infected chickens, including neurological disorders and immunosuppression. Most notably, MDV induces transformation of lymphocytes, leading to T cell lymphomas in visceral organs with a mortality of up to 100%. While several factors involved in MDV tumorigenesis have been identified, the transformation process and tumor composition remain poorly understood. Here we developed an imaging mass spectrometry (IMS) approach that allows sensitive visualization of MDV-induced lymphoma with a specific mass profile and precise differentiation from the surrounding tissue. To identify potential tumor markers in tumors derived from a very virulent wild-type virus and a telomerase RNA-deficient mutant, we performed laser capture microdissection (LCM) and thereby obtained tumor samples with no or minimal contamination from surrounding nontumor tissue. The proteomes of the LCM samples were subsequently analyzed by quantitative mass spectrometry based on stable isotope labeling. Several proteins, like interferon gamma-inducible protein 30 and a 70-kDa heat shock protein, were identified that are differentially expressed in tumor tissue compared to surrounding tissue and naive T cells. Taken together, our results demonstrate for the first time that MDV-induced tumors can be visualized using IMS, and we identified potential MDV tumor markers by analyzing the proteomes of virus-induced tumors.

IMPORTANCE Marek's disease virus (MDV) is an oncogenic alphaherpesvirus that infects chickens and causes the most frequent clinically diagnosed cancer in the animal kingdom. Not only is MDV an important pathogen that threatens the poultry industry but it is also used as a natural virus-host model for herpesvirus-induced tumor formation. In order to visualize MDV-induced lymphoma and to identify potential biomarkers in an unbiased approach, we performed imaging mass spectrometry (IMS) and noncontact laser capture microdissection. This study provides a first description of the visualization of MDV-induced tumors by IMS that could be applied also for diagnostic purposes. In addition, we identified and validated potential biomarkers for MDV-induced tumors that could provide the basis for future research on pathogenesis and tumorigenesis of this malignancy.

KEYWORDS Marek's disease virus, imaging mass spectrometry, lymphoma, noncontact laser capture microdissection, proteome, tumor, tumor markers

Marek's disease (MD) is caused by the oncogenic *Gallid alphaherpesvirus 2*, also known as Marek's disease virus (MDV). It is characterized by various clinical symptoms, including neurological disorders, immunosuppression, and most notably tumors in visceral organs (1). Remarkably, MD causes high economic losses in the

poultry industry worldwide and is used as a natural virus-host small-animal model for herpesvirus-induced cancers (2–4). MDV infection can cause mortality of up to 100% in susceptible chickens; however, the severity of disease and mortality are dependent on the genetic background of the host, vaccination status, and virulence of the virus strain (5). Upon infection of the host, MDV efficiently spreads to lymphoid organs and replicates in B and T cells. T cells are the target for the establishment of latency and transformation (6), while B cells have been recently shown to be dispensable for MDV pathogenesis (7). Most latently infected and transformed cells are CD4$^+$ T cells that rapidly replicate, resulting in the clinical signs and deadly lymphomas (8). These MDV-induced tumors efficiently develop in infected animals and can be observed as early as 3 to 4 weeks after infection (2). Several viral factors contribute to this rapid transformation as reviewed recently (9); these viral factors include the major oncoprotein Meq (2, 10, 11), the viral chemokine vIL-8 (12–14), MDV-encoded microRNAs (15–17), viral telomeric repeats (TMRs) (18–21), and a virus-encoded telomerase RNA (vTR) (22–25). For example, deletion of vTR severely impaired disease progression, tumor formation, and dissemination, while lytic replication was not affected (23, 26–28). Even though recent work has shed light on the role of vTR in MDV-induced tumor formation, many questions including whether tumor composition and markers differ in the absence of vTR, still remain unanswered. Recent advances in imaging mass spectrometry (IMS) techniques made it possible to link histological structures directly to mass spectrometric data (29). IMS has been used to visualize the distribution of a variety of biomolecules, including proteins with a wide molecular mass range, making it an extremely versatile tool. In the context of tumor biology, IMS allowed the identification of tumor markers from biopsy tissue sections (30). The proteins present in these tumor samples can be identified by additional mass spectrometry (MS) techniques. Biomarker candidates are subsequently validated by independent methods such as RT-qPCR. Until now, this approach had not been applied to MDV-induced tumors, and therefore, we lack reliable tumor markers. In this study, we applied IMS to MDV-induced lymphomas for the first time. We identified specific protein masses that were present in the tumor, but not the surrounding tissue. This allowed accurate visualization of tumors within healthy tissue and was furthermore confirmed by histochemistry. To identify potential tumor markers, we performed laser capture microdissection (LCM) on these tumor tissues. Several potential tumor markers were identified and confirmed by RT-qPCR.

RESULTS

MALDI imaging of MDV-induced lymphomas. To determine whether IMS is applicable for the detection of MDV-induced lymphomas, we analyzed sections of organs from MDV-infected chickens (Fig. 1). Lymphoma-specific mass signatures were readily identified in liver samples based on intact proteins with a mass range between 2,000 and 20,000 Da. Furthermore, we analyzed the peptides after proteolytic digestion of the tissue sections and scanned typical "peptide mass ranges" between 700 and 3,500 Da (Fig. 1F to J). Intriguingly, several identical lymphoma-specific masses were reliably detected in lymphomatous lesions that had developed in different organs obtained from different chickens (Fig. 1). Statistical evaluation of peptide spectra by cluster analysis revealed highly discriminative marker mass sets. Depending on the number of given clusters, the entire tumor was mapped as a single cluster, or some degree of differentiation within the tumor was revealed (Fig. 2), defining a region with specific expression profiles along the border of the tumor (Fig. 2C) or small islets with identical mass signatures that were interspersed within the tumor area (Fig. 2C and D). These results indicated that protein expression patterns for example at the margins of the tumor might differ from areas that are more central (Fig. 2B and C).

Laser-dissected tissue sections and mass spectrometry. To investigate the tumor tissue proteome in greater detail and to obtain potential tumor markers, we performed laser capture microdissection (LCM) on MDV-induced tumors and quantified the pro-
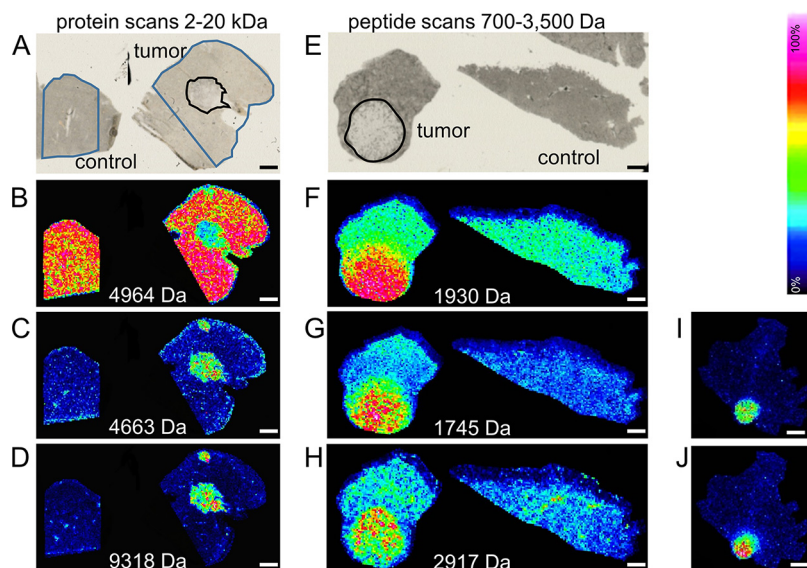
FIG 1 Protein and peptide IMS analysis of MDV-induced lymphomas. (A to D) Cryosections were prepared from the liver of a MDV-infected chicken, and an IMS protein scan was performed in the mass range between 2 and 20 kDa. The selected masses represent a marker for liver tissue (4,964 Da in panel B) and two for MDV-induced T cell tumors (4,663 Da and 9,318 Da in panels C and D, respectively). The remaining panels, panels E to J, show FFPE chicken liver (E to H) and chicken skeletal muscle (I and J) sections scanned in the typical peptide range (700 to 3,500 Da) after trypsin digestion of the sections. Panels A and E show HE-stained sections with or without (control) tumor; the regions that were measured by IMS are outlined in blue, and the tumor regions are outlined in black. IMS scans based on negative (B) and positive (C to D and F to H) tumor markers are shown. Panels I and J show the distributions of two tumor-specific masses (1,745 and 2,917 Da, respectively) that were identified in liver and skeletal muscle tumors from different animals. Intensities are rainbow color coded from 0% (black) to 100% (white) relative intensity according to the color code bar on the right. The represented masses are given for each panel. Bars, 1 mm.

tein content by mass spectrometry. MDV-induced lymphomas are solid and consist of a mixture of pleomorphic lymphocytes, including malignantly transformed T cells, reactive B and T cells, and also macrophages, that differ unequivocally from nonneoplastic tissue such as liver lobules (Fig. 1A), allowing the precise differentiation from surrounding nontransformed liver tissue. Samples were extracted from MDV-induced tumors (RB-1B strain) by LCM and lysed, and the protein content was quantified (10 to 15 μg of protein per sample). In addition, we analyzed tumors induced by a mutant MDV that lacks the telomerase RNA gene vTR (RB1B-ΔvTR) and that were more compact and mostly consisted of lymphocytes (see Fig. S1 in the supplemental material). For negative controls, we used primary nontransformed chicken T cells, the target cells of MDV transformation, as well as unaffected liver tissue in order to reduce false-positive results resulting from any remaining contamination. Two independent samples were isotope labeled by dimethylation, fractionated, and analyzed by LC-MALDI TOF/TOF MS. In total, about 1,000 proteins were reliably identified when comparing wild-type RB-1B (959 and 841 proteins) or RB1B-ΔvTR (1,314 or 919) tumors with primary chicken T cells.

Identification and confirmation of potential tumor markers. Next, we set out to determine differentially expressed proteins between tumor samples and naive T cells by quantitative MS based on introduced isotope labeling. In total, 19 promising potential transformation markers could be identified (Table 1 and Table S1) which were also differentially expressed when tumor samples were compared to healthy liver tissue samples. Eight proteins were upregulated and eleven were downregulated in MDV-induced tumors (wild-type RB-1B and RB1B-ΔvTR) compared to primary T cells and healthy liver controls. To confirm the potential transformation markers identified through our proteomic analysis, we assessed the mRNA levels of several randomly selected transformation markers in different tumor samples. RNA was isolated from
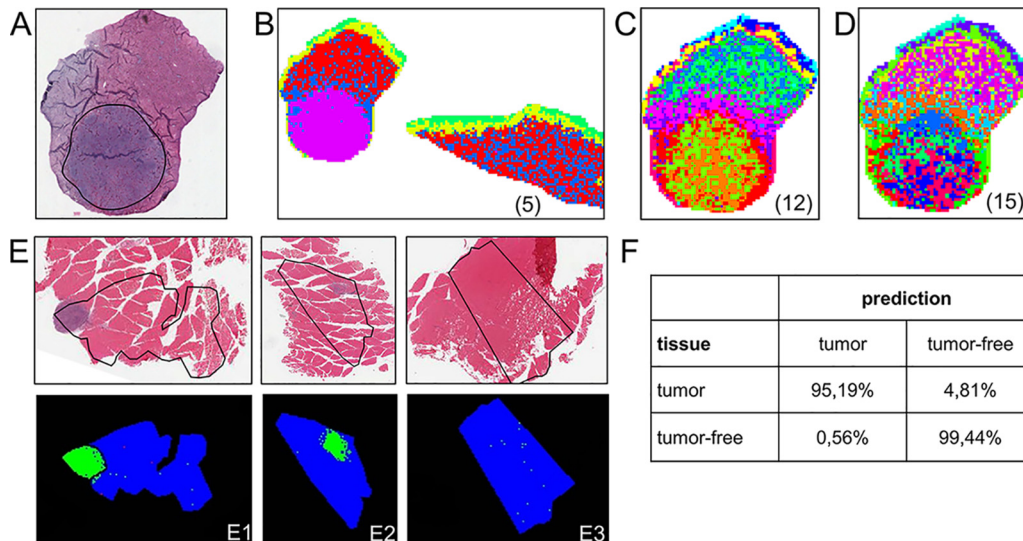
FIG 2 Statistical evaluation of MDV lymphoma peptide spectra. (A to D) Cluster analysis of spectra from a FFPE chicken liver section. (A) HE stain, the contour highlights the tumor region. (B) Joint cluster analysis of spectra from the section shown in panel A and a tumor-free control section with a given number of five clusters. Red and blue regions indicate tumor-free regions, which are clearly distinguished from the tumor appearing in magenta. Allowance of higher numbers of clusters as given in the parentheses in panels C and D resulted in a more fine-grained pattern. The margins of the tumor form a distinct red cluster in panel C, and the central region of the tumor shows microheterogeneity in, e.g., the green, dark blue, and red clusters in panel D. The color coding applies to each panel separately. The analysis was performed with in-house scripts using the statistical programming language R (63). (E1 to E3) Statistical models based on tumor-specific mass patterns of the chicken breast muscle tissue sample E1 were calculated using ClinProTools (Bruker) software. Spectra from the region outlined by the blue contour of the micrograph (E1) were used as training data for tumor (outlined in black) and tumor-free (outside the black outline) tissue. Models were then used to classify spectra from tissue sections of different animals that contained a tumor (E2) or were tumor-free controls (E3). Cross-validation of the models using the training data (E1) was correct for >99% of the data points. The regions predicted as tumor or tumor-free in the test sections E2 and E3 are shown in green and blue, respectively, and corresponded very well to the histological assessment of the sections (see Fig. S2 in the supplemental material). (F) The confusion matrix gives the prediction results of spectra from E2 and E3 in raster spots. In the tumor section, >95% of the area was correctly identified ($n = 416$), and prediction of the tumor-free region was correct for >99% ($n = 3,036$) showing that detection of MDV-induced tumors by IMS is feasible and exhibited high sensitivity and specificity.

laser-dissected material, healthy nontransformed tissue, and naive T cells and analyzed by RT-qPCR. All tested potential transformation markers could be confirmed by RT-qPCR (Table 1), with TAP1 as the only exception. IFI30, OASL, and a HSP70 were found to be upregulated in tumor samples as observed in the proteomic analysis (Table 1). Similarly, LBR, GSTT1L, RCC2, FYB, and H2AJF were downregulated on both the mRNA and protein level (Table 1). Taken together, we identified several potential tumor makers that in most cases could be confirmed by RT-qPCR.

DISCUSSION

The most prominent characteristic of MDV is the ability to transform T cells and cause lymphomas in infected animals. The onset of MDV-induced tumor development is very rapid and can occur within 3 to 4 weeks postinfection. MDV integrates its genome in latently infected and tumor cells, allowing maintenance of the viral genetic material in dividing cells (18, 19). The rapid replication that is mostly driven by the viral oncogenes ultimately leads to the fatal lymphoma formation in visceral organs (6). In this study, we developed an imaging mass spectrometry (IMS) approach to visualize MDV tumors and obtain a specific mass profile and accurate differentiation from the surrounding tissue. Intriguingly, differences regarding specific signatures at the margin and central area of the tumors were observed. Similar findings were recently described for the intratumoral microheterogeneity of myxoid sarcomas (31) and distinct expression profiles in the microenvironment of breast tumors (32), stressing the value of IMS as an "open-view" approach complementing the targeted analysis provided by classical histological techniques. Our data demonstrate that the derived signatures were specific

TABLE 1 Potential transformation markers

Ensembl accession no.	Protein (abbreviation)	Fold change[a] by:	
		MS	RT-qPCR
ENSGALP00000005345	Interferon gamma-inducible protein 30 (IFI30)	3.83	3.56
ENSGALP00000041758	Transporter 1 ATP-binding cassette subfamily B (TAP1)	3.26	0.78
ENSGALP00000010210	Leukocyte cell-derived chemotaxin 2 (LECT2)	2.82	
ENSGALP00000016536	Heat shock 70-kDa protein 4-like (HSP70)	2.53	1.42
ENSGALP00000028664	2'-5'-Oligoadenylate synthetase-like (OASL)	2.49	2.10
ENSGALP00000039235	Cold shock domain containing E1 (CSDE1)	2.39	
ENSGALP00000013029	Splicing factor 3b subunit 1 (SF3B1)	2.29	
ENSGALP00000042479	Stress-induced phosphoprotein 1 (STIP1)	2.23	
ENSGALP00000011961	Phosphatidylethanolamine binding protein 1 (PEBP1)	0.47	
ENSGALP00000016363	Heterochromatin protein 1 binding protein 3 (HP1BP3)	0.47	
ENSGALP00000015128	Lamin B receptor (LBR)	0.42	0.20
ENSGALP00000010358	p21 protein (Cdc42/Rac)-activated kinase 2 (PAK2)	0.41	
ENSGALP00000033650	FYN binding protein (FYB)	0.39	0.44
ENSGALP00000003584	H3 histone family 3B (H3F3B)	0.35	
ENSGALP00000039872	Regulator of chromosome condensation 2 (RCC2)	0.35	0.37
ENSGALP00000041526	Histone cluster 1 H4-VI germinal H4 mRNA (HIST1H4A)	0.34	
ENSGALP00000008341	Glutathione S-transferase theta 1-like (GSTT1L)	0.27	0.19
ENSGALP00000040653	H2A histone family member J (H2AFJ) mRNA	0.26	0.44
ENSGALP00000027541	High mobility group box 1 (HMGB1)	0.25	

[a]Fold changes by MS describe the relative expression of the proteins in the tumors in relation to the expression in T cells. Values of >2 indicate overexpression in the tumor, while values of <0.5 indicate stronger expression in the naive T cells. Mean values of the experiments with RB1B and RB1B-ΔvTR tumors are given. Fold change by RT-qPCR was calculated as $2^{\Delta CT}$. For a list of identified peptides corresponding to the regulated proteins, see Table S1 in the supplemental material.

and robust and may have diagnostic potential. In future studies, we will compare the signatures obtained to those of MD tumors caused by other MDV strains, ALV- and REV-induced tumors, and nonviral tumors in chickens. Moreover, we implemented a proteomic workflow with a strongly reduced risk of tissue contamination and, hence, increased sensitivity for biomarker identification. This workflow is based on laser capture microdissection (LCM) of MDV tumors and reference material, followed by proteome analysis based on quantitative mass spectrometry. After digestion of extracted proteins, the peptides from different samples were isotope coded by dimethylation, mixed at 1:1 ratios, and fractionated by off-gel isoelectric focusing (OG IEF) to reduce the complexity of the mixture and to improve resolution of the mass spectrometric analysis by LC-MALDI TOF/TOF MS. Proteomic analysis of microdissected MDV tumors compared to naive T cells and surrounding liver tissue samples identified only 19 potential transformation markers (Table 1), showing that the expression profiles of naive and MDV-transformed T cells are very similar. We assume that the low number of potential transformation markers that we have identified results mainly from the high purity of the analyzed tumor samples, which rules out false-positive results resulting from any contaminating nonneoplastic tissue (33–36). Most of the candidates could be confirmed by RT-qPCR, indicating that they may indeed play a role for transformation. With our workflow, we successfully addressed the issue of tumor sample contamination by surrounding tissue for the differential analysis of MD tumors, which is virtually unavoidable if macroscopically isolated tissues are analyzed. As a result of the proteomic analysis, eight proteins were seen upregulated, and eleven proteins were downregulated in MD tumors compared to T cells (Table 1). Surprisingly, we did not identify significant differences in the proteomes of RB1B- and RB1B-ΔvTR-induced tumors. This is very intriguing and suggests that the morphological differences are either due to changes in the RNA level or in proteins that are below the detection level. Several of the identified markers could also be verified on the transcript level by RT-qPCR (Table 1). Only one out of four markers, which were upregulated in the proteomic analysis, TAP1, could not be confirmed on the transcript level by RT-qPCR. However, it is well-known that mRNA and protein expression levels do not always correlate due to complex regulation of transcription, processing, and degradation of mRNA, translation, modification, and turnover of proteins, as well as the differences in

the half-lives of mRNA and proteins (37–40). Hence, it is possible that while the transcriptome is fully adapted to a certain condition, the proteome has not fully responded yet (38). The strongest upregulation that we could observe applied to IFI30, which has diverse cellular functions. It maintains the redox state of the cell, influencing autophagy, cellular activation, and proliferation. It has been shown that IFI30 is involved in the processing of epitopes from viral glycoproteins, for example, gB from herpes simplex virus 1 (HSV-1) and that it plays a role in eliciting an immune response toward HSV-1 infection (41). In addition, cancer infiltrating antigen-presenting cells elicit MHC II antigen processing and presentation through IFI30, shaping an antitumor T cell strategy (42). IFI30 may also influence tumorigenesis through alteration of the redox state, and cell proliferation (41). Taken together, IFI30 upregulation hints toward a host antitumor response. Upregulation of the molecular chaperone protein HSP70 has been identified previously in MDV-induced tumor cells, and there is very strong evidence that the interaction of Meq and HSP70 is significant in MDV lymphomagenesis (43). Similarly, the proteins OASL and TAP1 were upregulated in MD tumors. While OASL is an interferon-induced protein that regulates the early phase of viral infection, proviral functions like enhancement of viral persistence are also associated with members of the OAS family (44). Previous experiments have shown that the interferon gamma-induced pathway is altered in a MDV-transformed chicken $CD4^+$ T cell line, resembling activation of T cells (45). TAP1 is involved in MHC class I antigen presentation (46), and slight upregulation of TAP2 in the tips of feathers of MDV-infected chickens was reported previously (47). The upregulation of several immune response-associated proteins indicate an activation of T cells, which could enhance the proliferation of tumor cells. While several immune response-associated proteins were upregulated in MDV-induced lymphomas compared to T cells, proteins associated with transcription and nucleosome assembly were found to be downregulated, for example, RCC2 (48), H2AFJ (49), H3F3B (50), HP1BP3 (51), and LBR (52). This is consistent with microarray investigations of MDV transformation in chicken spleens where transcription-related processes were also found to be downregulated (53). Similarly, a proteomic analysis of MDV-infected chicken embryonic fibroblasts detected an increased presence of phosphoproteins in the nucleus, indicating an effect on transcription regulation (54). Furthermore, two of the downregulated proteins are associated with signaling pathways that regulate the cytoskeleton (FYB [55] and PAK2 [56]). Burgess et al. previously demonstrated that Hodgkin's disease antigen (CD30) is upregulated in tumors induced by HPRS-16 or GA/22 in line 7_2 and 6_1 chickens as well as Ross broilers (57, 58). We did not observe this CD30 upregulation in tumors induced by the very virulent RB-1B strain upon infection of Valo SPF chickens, suggesting that the virus strain and chicken line might influence the upregulation of CD30. In this study, we established a pipeline for efficient IMS and LCM of MDV-induced tumors and could identify highly discriminative marker mass sets for these tumors. This confirms that IMS is an "open view" tool that is neither restricted to a defined analyte nor limited by the availability of antibodies, fluorescent chromophores, or nucleic acid probes. Furthermore, we successfully applied LC-MALDI TOF/TOF MS to analyze dimethyl-labeled OG IEF-fractionated peptides isolated from MDV lymphoma tissue compared to naive T cells and healthy liver tissue. Changes in host protein expression during the transformation process were analyzed. Further functional analyses are necessary to confirm a role of the identified markers during MDV-induced transformation.

MATERIALS AND METHODS

Ethics statement. All animal work was conducted according to the national and international guidelines for humane use of animals. Animal experiments were approved by the Landesamt für Gesundheit und Soziales (LAGeSo) in Berlin, Germnay (approval number G0218/12 and T0245/14).

Animals, cells, and tumors. Specific-pathogen-free (SPF) white Leghorn eggs were obtained from Valo Biomedia (Osterholz-Scharmbeck, Germany), and chickens hatched in the animal facility of the Center for Infection Medicine, Berlin, Germany. Primary T cells were isolated from the thymuses of 6- to 11-week-old chickens by manual dissociation of the organ, followed by isolation of the cells by density gradient centrifugation as described previously (59, 60). T cells were pelleted and stored at −80°C prior to lysis. MDV-induced tumors were collected from birds infected with the BAC-derived very virulent

wild-type RB1B virus (GenBank accession no. EF523390.1) (19, 61) and the RB1B-ΔvTR mutant (27). Briefly, birds were infected intra-abdominally with 4,000 PFU of the respective virus and were monitored for disease signs throughout the experiment. Birds with clinical signs were euthanized, and tumorous tissues were collected from chickens between 41 and 82 dpi. Tissues were fixed in formalin and stored at 4°C or snap-frozen in liquid nitrogen and stored at −80°C.

MALDI imaging of MDV-induced lymphomas. Relevant locations for IMS imaging were selected based on hematoxylin-and-eosin (HE)-stained tissue sections. IMS on formalin-fixed paraffin-embedded tissue (FFPE) was performed following a published protocol (62) and the guidelines of the manufacturer of the MS platform (Bruker). To this end, tissues were cut at 5 μm and mounted on a conductive indium tin oxide (ITO)-coated glass slides (catalog no. 8237001; Bruker Daltonik GmbH) to avoid charge build-up during the measurement of mass spectra. For peptide measurements, the FFPE tissue sections were stored at 56°C overnight and dewaxed by immersing the slide in xylene and rehydration in a graded ethanol series on the following day. The antigens were demasked by heating the tissue sections in 10 mM Tris buffer (pH 9.0) for 10 min at 110°C in a decloaking chamber (Biocare Medical). Subsequently, peptides were liberated by digestion with trypsin (Promega) on the tissue. Both the enzyme and later the matrix were applied by an automatic sprayer (ImagePrep; Bruker), following standard protocols suggested by the manufacturer, resulting in a homogenous matrix layer over the whole tissue section. α-Cyano-4-hydroxycinnamic acid (HCCA) was used as matrix for peptide and protein analysis. Spectra were acquired with an Ultraflex MALDI-TOF/TOF mass spectrometer. The software projects a grid of spots over the region of interest, and from every spot, a spectrum is acquired. Obtained spectra were normalized before images were exported. Colored graphs in Fig. 1 show the distribution and relative intensity of a specific mass in rainbow color code. Statistical models were calculated using the ClinPro-Tools software (Bruker). For k-means cluster analysis, the peaklists of the spectra were exported to statistical software R (63) and processed with an in-house script. Peak alignments were calculated across all measured spectra using maximal bin sizes (mass tolerances) of 5,000 ppm with the R package caMassClass (version 1.9 [64]). Based on this matrix, k-means clustering was performed with a predefined number of clusters. For the graphic representation, images were reconstructed with the R package pixmap (version 04-11 [65]) using the clusters for color coding.

Laser capture microdissection (LCM). Frozen tumor tissues from two independent replicates per virus mutant were cut into 20-μm cryosections using a precooled HM 560 Cryostar cryostat (Microm International). Cryosections were fixed with ice-cold ethanol (70% for 1 min, followed by a dip in 100%) and dried prior to laser dissection for 1 h at RT in a mild vacuum (150 mm Hg). LCM was performed using the Palm MicroBeam system and the Palm RoboSoftware 4.5 (Zeiss) according to the manufacturer's instructions. For each tumor, 10 identical rectangles of 2.5 mm² each, equivalent to a total of approximately 10^4 cells, and 10 such cuts from unaffected tissue were collected. Tissue cuts were dried by vacuum centrifugation, lysed in 30 μl lysis buffer (0.1 M Tris-HCl [pH 8.0], 0.1 M DTT, and 2% SDS), heated for 10 min at 95°C, and sonicated. For a control, 1×10^7 chicken T cells were lysed in 100 μl lysis buffer. The supernatants were recovered for filter-aided sample preparation (FASP) digest as described previously (66). The protein contents of lysed samples were assessed by densitometry of Coomassie blue-stained SDS-PAGE gels with BSA standards (Merck) (67).

Protein labeling and LC-MALDI TOF/TOF mass spectrometry. Dimethyl labeling of peptides for the quantification of proteins in tumor tissue, unaffected liver tissue, and primary T cells was performed as described previously (68). Samples were desalted using Empore solid-phase extraction cartridges (3M) (66), mixed at 1:1 protein ratios, and fractionated by gel-free isoelectric focusing with an Agilent 3100 Offgel fractionator as described previously (69). Separated peptide fractions were further separated based on hydrophobicity on a LC column with the EASY-nLC II (Bruker) chromatographic system, spotted to a MALDI target (Proteineer fcII; Bruker), and analyzed in an UltrafleXtreme MALDI-TOF/TOF mass spectrometer (Bruker) as described previously (69). Peptide spectra were acquired in the *m/z* range 700 to 3,500 Da with a minimum signal-to-noise (S/N) ratio of 7. Proteins were identified on basis of the MS/MS with a Mascot server (version 2.4.1; Matrix Science [70]) and analyzed using ProteinScape software (version 3; Bruker). As sequence database, the *Gallus gallus* proteome downloaded from the ENSEMBL website (71) and the viral sequences were added to the FASTA file. Oxidation of methionine, acetylation of protein N′ termini, and dimethylation of lysine and peptide N′ termini (both isotopomeric forms) were set as variable modifications, whereas the carbamydomethylation of cysteine residues was set as a fixed modification. Up- and downregulated proteins were identified using ProteinScape (Bruker) and an in-house R script. Candidate protein markers showing at least twofold up- or downregulation were selected for confirmation by qPCR.

Confirmation of transformation markers by RT-qPCR. The RNA from cells and tissue sections was isolated with the RNeasy minikit (Qiagen) following the manufacturer's instructions. Several randomly selected potential transformation markers were confirmed using one-step RT-qPCR using the qScript one-step SYBR Green qRT-PCR kit (Quantabio) in an CFX96 Touch real-time PCR detection system (Bio-Rad). Samples were measured in duplicates, and expression levels were calculated relative to expression of GAPDH, 28S rRNA, and β-actin (Table 2) using the $2^{\Delta Ct}$ method as described previously (72).

Immunohistochemistry and quantitation of cell types. To assess morphology and tumor morphology, 3-μm-thick FFPE sections were prepared and HE stained according to standardized procedures. By immunohistochemistry, T cells were detected using a polyclonal rabbit anti-human CD3 antibody (catalog no. A0452; Dako) (1:200) and the Vectastain Elite ABC HRP detection kit (Vector Laboratories). CD3-positive and -negative round cells, assumed to be B cells and macrophages, were quantified in three independent tumors induced by wild-type RB1B or RB1B-ΔvTR using the Halo imaging software (Indica

TABLE 2 Primers used in this study for quantitative PCR to confirm *Gallus gallus* genes as potential transformation markers

NCBI reference sequence	Gene name	Primer sequence[a]	Product size (bp)
NM_205041.1	2′-5′-Oligoadenylate synthetase like (OASL)	For: 5′-AGGTCCTGGTGAAGGACAGT-3′ Rev: 5′-TCCAGCTCCTTGGTCTCGTA-3′	145
	28S RNA	For: 5′-GGTATGGGCCCGACGCT-3′ Rev: 5′-CCGATGCCGACGCTCAT-3′	144
NM_205518.1	Actin, beta (ACTB)	For: 5′-GAGAAATTGTGCGTGACATCA-3′ Rev: 5′-CCTGAACCTCTCATTGCCA-3′	152
NM_001031451.1	FYN binding protein (FYB)	For: 5′-GCCCCAAAACGGAAGTCTTTGC-3′ Rev: 5′-TGGGCTTGACATTTCTGGGCG-3′	256
XM_001231970.4	Glutathione S-transferase theta 1-like (GSTT1L)	For: 5′-AACAGGCCAGGGTTGATGAG-3′ Rev: 5′-AGCACCTTCCACTTTCTCCG-3′	137
NM_204305.1	Glyceraldehyde-3-phosphate dehydrogenase (GAPDH)	For: 5′-AATGGCTTTCCGTGTGCCAACC-3′ Rev: 5′-ATTCAGTGCAATGCCAGCACCC-3′	223
NM_001030753.1	H2A histone family, member J (H2AFJ)	For: 5′-AGGCCAAGTCGCGTTCATC-3′ Rev: 5′-ATCTCGGCCGTCAGGTACT-3′	148
NM_001012576.1	Heat shock protein family A (Hsp70) member 4-like (HSPA4L)	For: 5′-TGGCGACAACTCCAAAGTGA-3′ Rev: 5′-TCAGTATCCATCGCTGCGTC-3′	129
XM_418246.5	Interferon, gamma-inducible protein 30 (IFI30)	For: 5′-CGCTCAGGAGAGGAATGTCT-3′ Rev: 5′-GCAAGCCTTCAGATTCTTGG-3′	181
NM_205342.1	Lamin B receptor (LBR)	For: 5′-GCAAACAAGATGACCCCAGC-3′ Rev: 5′-GGCCTTCCACAACCTTTCCT-3′	150
M75729.1	MDV 175-kDa protein (ICP4) gene	For: 5-TTTCTAGCAAGGAGCGACGC-3′ Rev: 5-CTGACTTGCGCTTACGGGAA-3′	81
XM_015296999.1	Regulator of chromosome condensation 2 (RCC2)	For: 5′-CTGGTTGTAGGCTTGGAGCA-3′ Rev: 5′-TGAGGAAGGAGGGTGGGAAA-3′	146
NM_001135968.1	Transporter 1, ATP-binding cassette, subfamily B (MDR/TAP) (TAP1)	For: 5′-ACGACTTCATCACTCGCCTGC-3′ Rev: 5′-TCCAACACCACCACTCGTTGTG-3′	280

[a]For, forward primer; Rev, reverse primer.

Labs). Six randomly selected areas were quantified for each tumor, and healthy liver tissue sections were used as a control.

SUPPLEMENTAL MATERIAL

Supplemental material for this article may be found at https://doi.org/10.1128/mSphere.00569-18.

FIG S1, TIF file, 0.1 MB.
FIG S2, TIF file, 7.1 MB.
TABLE S1, DOCX file, 0.04 MB.

REFERENCES

1. Jarosinski KW, Tischer BK, Trapp S, Osterrieder N. 2006. Marek's disease virus: lytic replication, oncogenesis and control. Expert Rev Vaccines 5:761–772. https://doi.org/10.1586/14760584.5.6.761.
2. Calnek BW. 1998. Lymphomagenesis in Marek's disease. Avian Pathol 27:S54–S64. https://doi.org/10.1080/03079459808419293.
3. Osterrieder N, Kamil JP, Schumacher D, Tischer BK, Trapp S. 2006. Marek's disease virus: from miasma to model. Nat Rev Microbiol 4:283–294. https://doi.org/10.1038/nrmicro1382.
4. Calnek BW. 1986. Marek's disease–a model for herpesvirus oncology. Crit Rev Microbiol 12:293–320.
5. Witter RL. 1997. Increased virulence of Marek's disease virus field isolates. Avian Dis 41:149–163. https://doi.org/10.2307/1592455.
6. Nair V. 2013. Latency and tumorigenesis in Marek's disease. Avian Dis 57:360–365. https://doi.org/10.1637/10470-121712-Reg.1.
7. Bertzbach LD, Laparidou M, Hartle S, Etches RJ, Kaspers B, Schusser B, Kaufer BB. 2018. Unraveling the role of B cells in the pathogenesis of an

oncogenic avian herpesvirus. Proc Natl Acad Sci U S A 115:11603–11607. https://doi.org/10.1073/pnas.1813964115.

8. Schat KA, Chen CL, Calnek BW, Char D. 1991. Transformation of T-lymphocyte subsets by Marek's disease herpesvirus. J Virol 65: 1408–1413.

9. Bertzbach LD, Kheimar A, Ali FAZ, Kaufer BB. 2018. Viral factors involved in Marek's disease virus (MDV) pathogenesis. Curr Clin Microbiol Rep 5:238–244. https://doi.org/10.1007/s40588-018-0104-z.

10. Jones D, Lee L, Liu JL, Kung HJ, Tillotson JK. 1992. Marek disease virus encodes a basic-leucine zipper gene resembling the fos/jun oncogenes that is highly expressed in lymphoblastoid tumors. Proc Natl Acad Sci U S A 89:4042–4046. https://doi.org/10.1073/pnas.89.9.4042.

11. Lupiani B, Lee LF, Cui X, Gimeno I, Anderson A, Morgan RW, Silva RF, Witter RL, Kung HJ, Reddy SM. 2004. Marek's disease virus-encoded Meq gene is involved in transformation of lymphocytes but is dispensable for replication. Proc Natl Acad Sci U S A 101:11815–11820. https://doi.org/10.1073/pnas.0404508101.

12. Parcells MS, Lin SF, Dienglewicz RL, Majerciak V, Robinson DR, Chen HC, Wu Z, Dubyak GR, Brunovskis P, Hunt HD, Lee LF, Kung HJ. 2001. Marek's disease virus (MDV) encodes an interleukin-8 homolog (vIL-8): characterization of the vIL-8 protein and a vIL-8 deletion mutant MDV. J Virol 75:5159–5173. https://doi.org/10.1128/JVI.75.11.5159-5173.2001.

13. Cui XP, Lee LF, Reed WM, Kung HJ, Reddy SM. 2004. Marek's disease virus-encoded vIL-8 gene is involved in early cytolytic infection but dispensable for establishment of latency. J Virol 78:4753–4760. https://doi.org/10.1128/JVI.78.9.4753-4760.2004.

14. Engel AT, Selvaraj RK, Kamil JP, Osterrieder N, Kaufer BB. 2012. Marek's disease viral interleukin-8 promotes lymphoma formation through targeted recruitment of B cells and CD4+ CD25+ T cells. J Virol 86: 8536–8545. https://doi.org/10.1128/JVI.00556-12.

15. Yao Y, Nair V. 2014. Role of virus-encoded microRNAs in avian viral diseases. Viruses 6:1379–1394. https://doi.org/10.3390/v6031379.

16. Teng M, Yu ZH, Zhao P, Zhuang GQ, Wu ZX, Dang L, Li HZ, Ma SM, Cui ZZ, Zhang GP, Wu R, Luo J. 2017. Putative roles as oncogene or tumour suppressor of the Mid-clustered microRNAs in Gallid alphaherpesvirus 2 (GaHV2) induced Marek's disease lymphomagenesis. J Gen Virol 98: 1097–1112. https://doi.org/10.1099/jgv.0.000786.

17. Zhuang G, Sun A, Teng M, Luo J. 2017. A tiny RNA that packs a big punch: the critical role of a viral miR-155 ortholog in lymphomagenesis in Marek's disease. Front Microbiol 8:1169. https://doi.org/10.3389/fmicb.2017.01169.

18. Kaufer BB, Jarosinski KW, Osterrieder N. 2011. Herpesvirus telomeric repeats facilitate genomic integration into host telomeres and mobilization of viral DNA during reactivation. J Exp Med 208:605–615. https://doi.org/10.1084/jem.20101402.

19. Greco A, Fester N, Engel AT, Kaufer BB. 2014. Role of the short telomeric repeat region in Marek's disease virus replication, genomic integration, and lymphomagenesis. J Virol 88:14138–14147. https://doi.org/10.1128/JVI.02437-14.

20. Osterrieder N, Wallaschek N, Kaufer BB. 2014. Herpesvirus genome integration into telomeric repeats of host cell chromosomes. Annu Rev Virol 1:215–235. https://doi.org/10.1146/annurev-virology-031413-085422.

21. Kheimar A, Previdelli RL, Wight DJ, Kaufer BB. 2017. Telomeres and telomerase: role in Marek's disease virus pathogenesis, integration and tumorigenesis. Viruses 9:E173.

22. Fragnet L, Blasco MA, Klapper W, Rasschaert D. 2003. The RNA subunit of telomerase is encoded by Marek's disease virus. J Virol 77:5985–5996. https://doi.org/10.1128/JVI.77.10.5985-5996.2003.

23. Trapp S, Parcells MS, Kamil JP, Schumacher D, Tischer BK, Kumar PM, Nair VK, Osterrieder N. 2006. A virus-encoded telomerase RNA promotes malignant T cell lymphomagenesis. J Exp Med 203:1307–1317. https://doi.org/10.1084/jem.20052240.

24. Kaufer BB, Trapp S, Jarosinski KW, Osterrieder N. 2010. Herpesvirus telomerase RNA(vTR)-dependent lymphoma formation does not require interaction of vTR with telomerase reverse transcriptase (TERT). PLoS Pathog 6:e1001073. https://doi.org/10.1371/journal.ppat.1001073.

25. Chbab N, Egerer A, Veiga I, Jarosinski KW, Osterrieder N. 2010. Viral control of vTR expression is critical for efficient formation and dissemination of lymphoma induced by Marek's disease virus (MDV). Vet Res 41:56. https://doi.org/10.1051/vetres/2010026.

26. Kaufer BB, Arndt S, Trapp S, Osterrieder N, Jarosinski KW. 2011. Herpesvirus telomerase RNA (vTR) with a mutated template sequence abrogates herpesvirus-induced lymphomagenesis. PLoS Pathog 7:e1002333. https://doi.org/10.1371/journal.ppat.1002333.

27. Kheimar A, Kaufer BB. 2018. Epstein-Barr virus-encoded RNAs (EBERs) complement the loss of Herpesvirus telomerase RNA (vTR) in virus-induced tumor formation. Sci Rep 8:209. https://doi.org/10.1038/s41598-017-18638-7.

28. Kheimar A, Trimpert J, Groenke N, Kaufer BB. 2018. Overexpression of cellular telomerase RNA enhances virus-induced cancer formation. Oncogene https://doi.org/10.1038/s41388-018-0544-1.

29. Angel PM, Caprioli RM. 2013. Matrix-assisted laser desorption ionization imaging mass spectrometry: in situ molecular mapping. Biochemistry 52:3818–3828. https://doi.org/10.1021/bi301519p.

30. Schone C, Hofler H, Walch A. 2013. MALDI imaging mass spectrometry in cancer research: combining proteomic profiling and histological evaluation. Clin Biochem 46:539–545. https://doi.org/10.1016/j.clinbiochem.2013.01.018.

31. Willems SM, van Remoortere A, van Zeijl R, Deelder AM, McDonnell LA, Hogendoorn PC. 2010. Imaging mass spectrometry of myxoid sarcomas identifies proteins and lipids specific to tumour type and grade, and reveals biochemical intratumour heterogeneity. J Pathol 222:400–409. https://doi.org/10.1002/path.2771.

32. Kang S, Maeng H, Kim BG, Qing GM, Choi YP, Kim HY, Kim PS, Kim Y, Kim YH, Choi YD, Cho NH. 2012. In situ identification and localization of IGHA2 in the breast tumor microenvironment by mass spectrometry. J Proteome Res 11:4567–4574. https://doi.org/10.1021/pr3003672.

33. Lu Z, Qin A, Qian K, Chen X, Jin W, Zhu Y, Eltahir YM. 2010. Proteomic analysis of the host response in the bursa of Fabricius of chickens infected with Marek's disease virus. Virus Res 153:250–257. https://doi.org/10.1016/j.virusres.2010.08.010.

34. Thanthrige-Don N, Parvizi P, Sarson AJ, Shack LA, Burgess SC, Sharif S. 2010. Proteomic analysis of host responses to Marek's disease virus infection in spleens of genetically resistant and susceptible chickens. Dev Comp Immunol 34:699–704. https://doi.org/10.1016/j.dci.2010.01.016.

35. Hu X, Qin A, Qian K, Shao H, Yu C, Xu W, Miao J. 2012. Analysis of protein expression profiles in the thymus of chickens infected with Marek's disease virus. Virol J 9:256. https://doi.org/10.1186/1743-422X-9-256.

36. Jie H, Lian L, Qu LJ, Zheng JX, Hou ZC, Xu GY, Song JZ, Yang N. 2013. Differential expression of Toll-like receptor genes in lymphoid tissues between Marek's disease virus-infected and noninfected chickens. Poult Sci 92:645–654. https://doi.org/10.3382/ps.2012-02747.

37. Nagaraj N, Wisniewski JR, Geiger T, Cox J, Kircher M, Kelso J, Paabo S, Mann M. 2011. Deep proteome and transcriptome mapping of a human cancer cell line. Mol Syst Biol 7:548. https://doi.org/10.1038/msb.2011.81.

38. Vogel C, Marcotte EM. 2012. Insights into the regulation of protein abundance from proteomic and transcriptomic analyses. Nat Rev Genet 13:227–232. https://doi.org/10.1038/nrg3185.

39. Skiba M, Glowinski F, Koczan D, Mettenleiter TC, Karger A. 2010. Gene expression profiling of Pseudorabies virus (PrV) infected bovine cells by combination of transcript analysis and quantitative proteomic techniques. Vet Microbiol 143:14–20. https://doi.org/10.1016/j.vetmic.2010.02.009.

40. Liu Y, Beyer A, Aebersold R. 2016. On the dependency of cellular protein levels on mRNA abundance. Cell 165:535–550. https://doi.org/10.1016/j.cell.2016.03.014.

41. West LC, Cresswell P. 2013. Expanding roles for GILT in immunity. Curr Opin Immunol 25:103–108. https://doi.org/10.1016/j.coi.2012.11.006.

42. Rausch MP, Hastings KT. 2015. Diverse cellular and organismal functions of the lysosomal thiol reductase GILT. Mol Immunol 68:124–128. https://doi.org/10.1016/j.molimm.2015.06.008.

43. Zhao Y, Kurian D, Xu H, Petherbridge L, Smith LP, Hunt L, Nair V. 2009. Interaction of Marek's disease virus oncoprotein Meq with heat-shock protein 70 in lymphoid tumour cells. J Gen Virol 90:2201–2208. https://doi.org/10.1099/vir.0.012062-0.

44. Choi UY, Kang JS, Hwang YS, Kim YJ. 2015. Oligoadenylate synthase-like (OASL) proteins: dual functions and associations with diseases. Exp Mol Med 47:e144. https://doi.org/10.1038/emm.2014.110.

45. Buza JJ, Burgess SC. 2008. Different signaling pathways expressed by chicken naive CD4+ T cells, CD4+ lymphocytes activated with staphylococcal enterotoxin B, and those malignantly transformed by Marek's disease virus. J Proteome Res 7:2380–2387. https://doi.org/10.1021/pr700844z.

46. Walker BA, Hunt LG, Sowa AK, Skjodt K, Gobel TW, Lehner PJ, Kaufman J. 2011. The dominantly expressed class I molecule of the chicken MHC is explained by coevolution with the polymorphic peptide transporter

(TAP) genes. Proc Natl Acad Sci U S A 108:8396–8401. https://doi.org/10.1073/pnas.1019496108.

47. Abdul-Careem MF, Hunter BD, Sarson AJ, Parvizi P, Haghighi HR, Read L, Heidari M, Sharif S. 2008. Host responses are induced in feathers of chickens infected with Marek's disease virus. Virology 370:323–332. https://doi.org/10.1016/j.virol.2007.09.013.

48. Yenjerla M, Panopoulos A, Reynaud C, Fotedar R, Margolis RL. 2013. TD-60 is required for interphase cell cycle progression. Cell Cycle 12:837–841. https://doi.org/10.4161/cc.23821.

49. Nishida H, Suzuki T, Tomaru Y, Hayashizaki Y. 2005. A novel replication-independent histone H2a gene in mouse. BMC Genet 6:10. https://doi.org/10.1186/1471-2156-6-10.

50. Witt O, Albig W, Doenecke D. 1997. Transcriptional regulation of the human replacement histone gene H3.3B. FEBS Lett 408:255–260. https://doi.org/10.1016/S0014-5793(97)00436-5.

51. Liu H, Liang C, Kollipara RK, Matsui M, Ke X, Jeong BC, Wang Z, Yoo KS, Yadav GP, Kinch LN, Grishin NV, Nam Y, Corey DR, Kittler R, Liu Q. 2016. HP1BP3, a chromatin retention factor for co-transcriptional microRNA processing. Mol Cell 63:420–432. https://doi.org/10.1016/j.molcel.2016.06.014.

52. Olins AL, Rhodes G, Welch DB, Zwerger M, Olins DE. 2010. Lamin B receptor: multi-tasking at the nuclear envelope. Nucleus 1:53–70. https://doi.org/10.4161/nucl.1.1.10515.

53. Dang L, Teng M, Li HW, Li HZ, Ma SM, Zhao P, Li XJ, Deng RG, Zhang GP, Luo J. 2017. Dynamic changes in the splenic transcriptome of chickens during the early infection and progress of Marek's disease. Sci Rep 7:11648. https://doi.org/10.1038/s41598-017-11304-y.

54. Ramaroson MF, Ruby J, Goshe MB, Liu HC. 2008. Changes in the Gallus gallus proteome induced by Marek's disease virus. J Proteome Res 7:4346–4358. https://doi.org/10.1021/pr800268h.

55. Lee KW, Bode AM, Dong Z. 2011. Molecular targets of phytochemicals for cancer prevention. Nat Rev Cancer 11:211–218. https://doi.org/10.1038/nrc3017.

56. Wang S, Wilkes MC, Leof EB, Hirschberg R. 2010. Noncanonical TGF-beta pathways, mTORC1 and Abl, in renal interstitial fibrogenesis. Am J Physiol Renal Physiol 298:F142–F149. https://doi.org/10.1152/ajprenal.00320.2009.

57. Burgess SC, Young JR, Baaten BJ, Hunt L, Ross LN, Parcells MS, Kumar PM, Tregaskes CA, Lee LF, Davison TF. 2004. Marek's disease is a natural model for lymphomas overexpressing Hodgkin's disease antigen (CD30). Proc Natl Acad Sci U S A 101:13879–13884. https://doi.org/10.1073/pnas.0305789101.

58. Kumar S, Kunec D, Buza JJ, Chiang HI, Zhou H, Subramaniam S, Pendarvis K, Cheng HH, Burgess SC. 2012. Nuclear factor kappa B is central to Marek's disease herpesvirus induced neoplastic transformation of CD30 expressing lymphocytes in-vivo. BMC Syst Biol 6:123. https://doi.org/10.1186/1752-0509-6-123.

59. Martin A, Lillehoj HS, Kaspers B, Bacon LD. 1993. Antigen-specific T cell proliferation following coccidia infection. Poult Sci 72:2084–2094. https://doi.org/10.3382/ps.0722084.

60. Schermuly J, Greco A, Hartle S, Osterrieder N, Kaufer BB, Kaspers B. 2015. In vitro model for lytic replication, latency, and transformation of an oncogenic alphaherpesvirus. Proc Natl Acad Sci U S A 112:7279–7284. https://doi.org/10.1073/pnas.1424420112.

61. Petherbridge L, Brown AC, Baigent SJ, Howes K, Sacco MA, Osterrieder N, Nair VK. 2004. Oncogenicity of virulent Marek's disease virus cloned as bacterial artificial chromosomes. J Virol 78:13376–13380. https://doi.org/10.1128/JVI.78.23.13376-13380.2004.

62. Casadonte R, Caprioli RM. 2011. Proteomic analysis of formalin-fixed paraffin-embedded tissue by MALDI imaging mass spectrometry. Nat Protoc 6:1695–1709. https://doi.org/10.1038/nprot.2011.388.

63. R Development Core Team. 2011. R: a language and environment for statistical computing. R Foundation for Statistical Computing, Vienna, Austria. https://www.r-project.org.

64. Tuszynski J. 2010. caMassClass: processing & classification of protein mass spectra (SELDI) data. R package version 1.9. http://cran.r-project.org/package=caMassClass.

65. Bivand R, Leisch F, Maechler M. 2011. pixmap: bitmap images ("pixel maps"). R package version 0.4-11.

66. Wiśniewski JR, Zougman A, Nagaraj N, Mann M. 2009. Universal sample preparation method for proteome analysis. Nat Methods 6:359–362. https://doi.org/10.1038/nmeth.1322.

67. Spath PJ, Koblet H. 1979. Properties of SDS-polyacrylamide gels highly cross-linked with N,N'-diallyltartardiamide and the rapid isolation of macromolecules from the gel matrix. Anal Biochem 93:275–285. https://doi.org/10.1016/S0003-2697(79)80152-9.

68. Boersema PJ, Raijmakers R, Lemeer S, Mohammed S, Heck AJ. 2009. Multiplex peptide stable isotope dimethyl labeling for quantitative proteomics. Nat Protoc 4:484–494. https://doi.org/10.1038/nprot.2009.21.

69. Henning AK, Groschup MH, Mettenleiter TC, Karger A. 2014. Analysis of the bovine plasma proteome by matrix-assisted laser desorption/ionisation time-of-flight tandem mass spectrometry. Vet J 199:175–180. https://doi.org/10.1016/j.tvjl.2013.10.029.

70. Perkins DN, Pappin DJ, Creasy DM, Cottrell JS. 1999. Probability-based protein identification by searching sequence databases using mass spectrometry data. Electrophoresis 20:3551–3567. https://doi.org/10.1002/(SICI)1522-2683(19991201)20:18<3551::AID-ELPS3551>3.0.CO;2-2.

71. Aken BL, Achuthan P, Akanni W, Amode MR, Bernsdorff F, Bhai J, Billis K, Carvalho-Silva D, Cummins C, Clapham P, Gil L, Giron CG, Gordon L, Hourlier T, Hunt SE, Janacek SH, Juettemann T, Keenan S, Laird MR, Lavidas I, Maurel T, McLaren W, Moore B, Murphy DN, Nag R, Newman V, Nuhn M, Ong CK, Parker A, Patricio M, Riat HS, Sheppard D, Sparrow H, Taylor K, Thormann A, Vullo A, Walts B, Wilder SP, Zadissa A, Kostadima M, Martin FJ, Muffato M, Perry E, Ruffier M, Staines DM, Trevanion SJ, Cunningham F, Yates A, Zerbino DR, Flicek P. 2017. Ensembl 2017. Nucleic Acids Res 45:D635–D642. https://doi.org/10.1093/nar/gkw1104.

72. Lian L, Qu LJ, Sun HY, Chen YM, Lamont SJ, Liu CJ, Yang N. 2012. Gene expression analysis of host spleen responses to Marek's disease virus infection at late tumor transformation phase. Poult Sci 91:2130–2138. https://doi.org/10.3382/ps.2012-02226.